

# Low-Luminosity Extragalactic Water Masers toward M82, M51, and NGC4051

Yoshiaki Hagiwara

*National Astronomical Observatory of Japan, Tokyo, Japan*

yoshiaki.hagiwara@nao.ac.jp

## ABSTRACT

Sub-arcsecond observations using the Very Large Array (VLA) are presented of low-luminosity H<sub>2</sub>O maser emission in M82, M51, and NGC4051. New maser features have been detected within the M82 starburst complex. They are largely associated with star-forming activity such as optically-identified starburst-driven winds, H II regions, or the early phase of star-formation in the galaxy. H<sub>2</sub>O maser in M51 consists of blue- and red-shifted features relative to the systemic velocity of the galaxy. The red-shifted features are measured at the northwest of the nuclear radio source, while the location of the blue-shifted counterpart is displaced by  $\sim 2''$  from the radio source. A small velocity gradient closely aligned with the radio jet is detected from the red-shifted features. The red-shifted maser most likely amplifies the background radio continuum jet, while the blue-shifted counterpart marks off-nuclear star-formation in the galaxy. All of the detected maser features in the narrow-line Seyfert 1 galaxy NGC4051 remain unresolved by new VLA observations. Due to the low luminosity of the maser, the maser excitation is not directly related to the active galactic nucleus.

*Subject headings:* galaxies: active — galaxies: ISM — galaxies: individual: M 82, M 51, NGC 4051

## 1. INTRODUCTION

Since the discovery of the first 22 GHz extragalactic H<sub>2</sub>O maser towards M33 by Churchwell et al. (1977), significant progress in studies of extra-galactic H<sub>2</sub>O masers has been made, with the first detection of a nuclear H<sub>2</sub>O maser toward an active galactic nucleus (AGN) in NGC 4945 (Dos Santos & Lépine 1979). A number of single-dish surveys searching for new H<sub>2</sub>O masers in active galaxies have been conducted since, in which more than 1000 galaxies were observed. These surveys were stimulated by the VLBI imaging of H<sub>2</sub>O maser components in a sub-parsec-scale thin, warped, edge-on disk displaying Keplerian rotation around the nucleus of the Seyfert 2 galaxy NGC 4258 (e.g., Herrnstein et al. 1998). These surveys have increased the total number of extra-galactic H<sub>2</sub>O masers to  $\sim 80$  at present (Henkel et al. 2005; Kondratko et al. 2006).

It is generally recognized that extra-galactic

H<sub>2</sub>O masers can be grouped according to their isotropic luminosity ( $L_{\text{iso}}$ ) (e.g., Greenhill et al. 1993). High-luminosity ( $L_{\text{iso}} > 10 L_{\odot}$ ) H<sub>2</sub>O masers are associated with active nuclei. Low-luminosity ( $L_{\text{iso}} < 10 L_{\odot}$ ) H<sub>2</sub>O masers are mostly associated with star-forming activity however, some of them may also contain or be in low radio luminosity AGNs. The luminosities of Galactic H<sub>2</sub>O masers that are commonly observed in the envelopes of evolved stars and star-forming regions range, typically, from 0.001  $L_{\odot}$  to 1  $L_{\odot}$ , and no H<sub>2</sub>O maser with a luminosity well above 1  $L_{\odot}$  has ever been found our galaxy. Accordingly, H<sub>2</sub>O masers observed in nearby star-forming or starburst galaxies such as M33, M82, NGC253, and NGC6946 with  $L_{\text{iso}}$  values of 0.01–1  $L_{\odot}$  (e.g., Churchwell et al. 1977; Claussen et al. 1984; Ho et al. 1987; Baudry & Brouillet 1996) are most likely to originate in star-forming activity in the host galaxy. On the other hand, there has been debate over the nature of a sub-

population of  $\text{H}_2\text{O}$  masers with luminosities of  $1 L_\odot \lesssim L_{\text{iso}} \lesssim 10 L_\odot$ , most of which are considered to arise in prominent sites of star-formation or starburst-activity in galaxies. However, some of their host galaxies show AGN activity; low-luminosity water masers have been detected towards LINER or type 1 Seyfert nuclei in recent sensitive single-dish surveys (Henkel et al. 2002; Hagiwara et al. 2003; Braatz et al. 2004). They could simply be low-luminosity analogues of the high-luminosity masers in narrow-line AGNs such as LINERs and type 2 Seyferts, and lower maser luminosities might be explained by a close to face-on view of obscuring structure around the nucleus, such as a disk or torus in the line of sight, or a misalignment between the disk and a nuclear continuum in the line of sight (Hagiwara et al. 2003). It is important to explore the sub-population of extragalactic masers with  $1 L_\odot \lesssim L_{\text{iso}} \lesssim 10 L_\odot$  at high angular resolution, as they could advance the study of extra-galactic star-formation or probe the nuclei in low radio luminosity AGNs.

M82 ( $D = 3.63 \text{ Mpc}$ ; Freedman et al. (1994)) is a well-known nearby starburst galaxy with a long observing history at various wavelengths. The galaxy hosts a number of exotic radio sources within its starburst complex, including main- and satellite-line OH masers and absorption, which trace cold molecular material in the galaxy (e.g., Seaquist et al. 1997; McDonald et al. 2002). Several low-luminosity  $\text{H}_2\text{O}$  maser features were detected at  $1.4''$  resolution in earlier Very Large Array (VLA) observations (Baudry & Brouillet 1996) however, the resolution was not sufficient to pin down or resolve the maser to investigate its association with radio continuum sources such as the nucleus, jet, compact H II regions, or supernova remnants (SNRs).

The Whirlpool galaxy, M51 ( $D = 9.6 \text{ Mpc}$ ; Sandage & Tammann (1975)), has provided an ideal laboratory for studying molecular materials in a galactic star-forming environment. These materials are more abundant in the spiral arms than in the central region. The nuclear region is very complex, showing molecular emission that is asymmetric in both position and velocity with respect to the nucleus: the dominant red-shifted emission peak is  $1''$  to the west of the radio/optical nucleus (e.g., Scoville & Young 1983; Scoville et al. 1998). Ho et al. (1987) first reported

the discovery of low-luminosity  $\text{H}_2\text{O}$  maser emission towards the galaxy. A snapshot observation pin-pointed the location of the known red-shifted maser features (Hagiwara et al. 2001) northwest of the continuum peak of the galaxy, while the blue-shifted feature(s) have not previously been measured. Due to the insufficient velocity coverage of the earlier observation, the overall distribution of the maser emission has not yet been explored in detail.

NGC4051 ( $D = 9.7 \text{ Mpc}$ ; Adams (1977)) is known to be a narrow-line Seyfert 1 galaxy (NLS1) showing ‘broad’ emission line in  $\text{H}\beta$  ( $\text{FWHM} < 2000 \text{ km s}^{-1}$ ), narrower than that typically observed ( $\text{FWHM} = 2000\text{--}10000 \text{ km s}^{-1}$ ) towards broad-line Seyfert 1 galaxies (Osterbrock & Pogge 1985). NLS1s are characterized by their housing of low-mass black holes radiating near their Eddington limits (e.g., Williams et al. 2004). NGC4051 exhibits very strong X-ray intensity variability on many different timescales (e.g., Lawrence et al. 1987), which is interpreted as a result of its nuclear activity and extended starburst components dominated by soft X-ray emission (Singh 1999). Hagiwara et al. (2003) detected an  $\text{H}_2\text{O}$  maser in NGC4051 and identified it towards the center of the galaxy with a complex nuclear radio structure (e.g., Ulvestad & Wilson 1984). The maser luminosity is estimated to be  $\sim 2 L_\odot$ . The maser features span  $\sim 300 \text{ km s}^{-1}$  and straddle the systemic velocity of  $V_{\text{LSR}} = 730 \pm 3 \text{ km s}^{-1}$  (Hagiwara et al. 2003) nearly symmetrically. These Doppler-shifted maser features appear to indicate the presence of a rotating disk however, there has been no compelling evidence found to support the presence of a disk (Hagiwara et al. 2003). The origin of low-luminosity  $\text{H}_2\text{O}$  masers in NLS1s, including NGC 4051, remains unexplored.

In this paper, I report sub-arcsecond imaging of  $\text{H}_2\text{O}$  masers towards these three nearby galaxies, in order to update the earlier observations with higher resolution and sensitivity and to further explore the nature of low-luminosity masers. All of them are so weak (flux density  $< 100 \text{ mJy}$ ) that they cannot be studied in VLBI observations. Thus, sub-arcsecond imaging is currently the best method to resolve the masers. In section 5 the statistical infra-red and radio properties of the  $\text{H}_2\text{O}$  masers are discussed. Throughout this paper  $H_0 = 75 \text{ km s}^{-1}\text{Mpc}^{-1}$  is adopted.

## 2. OBSERVATIONS

Spectral line observations at 22 GHz using the NRAO<sup>1</sup> VLA were carried out for measurement of H<sub>2</sub>O maser emission (6<sub>16</sub>-5<sub>23</sub> transition) towards three nearby galaxies M82, M 51, and NGC4051 from 2002–2003. All the observations were performed on these galaxies when the array was in the A Configuration. All the observations were made by employing two intermediate frequency (IF) bands of width 12.5 or 6.25 MHz with a single polarization, divided into 32 or 64 spectral channels, yielding velocity resolutions of 1.32 or 2.63 km s<sup>-1</sup> per channel. Each IF band was centered on a velocity selected to cover all the maser emission, with respect to the local standard of rest (LSR).

Because low-luminosity extragalactic maser emission is difficult to detect within an atmospheric coherence time at 22 GHz, phase-referencing observations were employed, using a nearby calibrator source (Table 1) several degrees away from each galaxy. The observations were thus performed by switching to the phase-referencing source, typically every 2 minutes for 30 s. Amplitude and bandpass calibration were performed using observations of 3C286, and the flux density scale was estimated to be accurate to within 10%. The data were calibrated and mapped in the standard way using the NRAO Astronomical Image Processing Software (AIPS). A summary of the observations, including IF velocity ranges, synthesized beam dimensions, and rms noise for each observing run, is provided in Table 1. After the phase and amplitude calibrations, the image cube was continuum subtracted using channels with no significant line emission in order to obtain only the line-emission. Thus, the maser emission in M 82 was separated out from the continuum emission. The continuum image of M 82 was produced, collecting only line-free channels within a single 6.25 MHz IF band. In the (*u*, *v*) data of M 51 and NGC 4051, no continuum emission was detected to a 3  $\sigma$  rms noise level of 0.6 mJy beam<sup>-1</sup> for M 51, and 0.48 mJy beam<sup>-1</sup> for NGC 4051.

In this paper, the B1950.0 coordinate system is

<sup>1</sup>The National Radio Astronomy Observatory (NRAO) is operated by Associated Universities, Inc., under a cooperative agreement with the National Science Foundation.

adopted for the observations and figures of M82, since this system was used in many earlier works on M82 in the literature.

## 3. RESULTS

### 3.1. M82

Figure 1 shows the locations of the detected H<sub>2</sub>O masers, and other known sources in M82. A single-dish spectrum and individual VLA spectra of the H<sub>2</sub>O masers are displayed in Figures 2 and 3. All five VLA spectra had detections above the  $\sim 5\sigma$  level. However, one might suggest that the detected features at N2 and N3 need to be confirmed. All of these maser features remained unresolved at the angular resolution of  $\sim 93$  mas, corresponding to 1.7 pc at the adopted distance, in the robust weighted maps.

The entire galaxy was searched, and no other water maser emission was found in the velocity range of  $V_{\text{LSR}} = 50\text{--}150$  km s<sup>-1</sup>. The known redshifted emission (e.g., Claussen et al. 1984) in the galaxy was not seen in this observation. In addition to the four masers S1–S4 (using the designation by Baudry & Brouillet (1996)), detected with the VLA in the C-configuration at 1.4'' resolution (Baudry & Brouillet 1996), three maser sources are newly detected in our observing run (Fig. 3). They are hereafter labeled N1, N2, and N3, respectively. None of the positions of the H<sub>2</sub>O masers coincide with those of the OH masers, luminous X-ray sources, and infrared peaks that have been measured to date.

Table 2 shows the positions, peak flux intensities, velocities, and velocity widths of the detected masers at the highest angular resolution of 0.93''. These new maser positions are constrained better than those at 1.4'' resolution measured with the VLA in the C configuration by Baudry & Brouillet (1996). The shapes of the detected maser spectra that were reported in Baudry & Brouillet (1996) were relatively unchanged since their observation in 1993. The positions of S1 and S2 are consistent to within 0.08'' between the two observations, and the difference is most likely due to different interferometer beam sizes. No maser emission at or near the location of S3 and S4 was detected to a 3  $\sigma$  level of 3.3 mJy beam<sup>-1</sup> in this observation, probably due to intensity variation of the

maser. Table 2 lists the positions of the maser features at S2, in which the emission profile is peaked at several velocities, spanning  $\approx 30 \text{ km s}^{-1}$ , but all lying in an  $\sim 0.01''$  region centered on R.A. (B1950)= $09^{\text{h}}51^{\text{m}}42.1812^{\text{s}}$ , decl. (B1950)= $69^{\circ}54'59.260''$ .

Table 3 lists the nearest discrete continuum source and radio recombination line (RRL) for each  $\text{H}_2\text{O}$  maser. In order to compare the positions between the masers and discrete continuum sources in the literature (McDonald et al. 2002, and references therein), the published positions of two known sources at 15 GHz were adjusted to those on our 22 GHz continuum map, which led to a sensible shift of  $< 0.05''$  for  $41.95+57.5$  and  $43.30+59.2$ . Therefore, one can estimate that positions between the two observations can be compared at an accuracy of  $< 0.05''$ . The maser positions in Table 3 show an offset of  $0.2\text{--}0.3''$  (corresponding to  $0.36\text{--}0.54 \text{ pc}$ ) from the nearest continuum peaks. Such a large separation makes it difficult to conclude that the detected maser is associated with an  $\text{H II}$  region or SNR. Thus, the masers are not essentially associated with any continuum source at this resolution. Alternatively, (compact)  $\text{H II}$  regions were not detected due to the sensitivity limit of these observations.

### 3.2. M51

Figure 4 displays VLA spectra of  $\text{H}_2\text{O}$  masers detected towards the central region of M51. The red-shifted features, spanning  $V_{\text{LSR}} = 538 - 586 \text{ km s}^{-1}$ , were previously detected in VLA snapshot observations (Hagiwara et al. 2001). One of the known blue-shifted features, peaking at  $V_{\text{LSR}} = 445 \text{ km s}^{-1}$ , is detected by interferometry for the first time. These Doppler-shifted velocity features straddle the systemic velocity ( $V_{\text{sys,LSR}} = 472 \pm 3 \text{ km s}^{-1}$ ; Scoville & Young (1983)) of the galaxy.

Figure 5 shows the approximate locations of the blue- and red-shifted features on the 8.4 GHz VLA-A image of Bradley, Kaiser, & Baan (2004). None of these features is resolved by the uniformly weighted beam of  $82 \times 77 \text{ mas}^2$ . Assuming the masers have Gaussian distributions, the beam-deconvolved size of the red-shifted maser is  $\sim 25 \text{ mas}$ , corresponding to  $1.2 \text{ pc}$  at the accepted distance to the galaxy. The positions of all the detected red-shifted features are within

$0.01''$ , centered on R.A. (J2000)= $13^{\text{h}}29^{\text{m}}52^{\text{s}}.709$ , decl. (J2000)= $+47^{\circ}11'42''.79$ , which is consistent with the earlier observation by Hagiwara et al. (2001). The blue-shifted feature is located at R.A. (J2000.0)= $13^{\text{h}}29^{\text{m}}52^{\text{s}}.549$ , decl. (J2000.0)= $+47^{\circ}11'43''.34$ . The parameters of the maser features are listed in Table 4.

The projected distance between the blue- and red-shifted features corresponds to  $82 \text{ pc}$  (or  $1.7''$ ); the blue-shifted feature is well separated from the other known features and so they are not kinematically related. On the other hand, in both this and the earlier VLA observation, the red-shifted features are observed  $\sim 180 \text{ mas}$  (or  $8.6 \text{ pc}$ ) northwest of the radio continuum peak of the galaxy (Hagiwara et al. 2001), suggesting that the maser does arise from the radio jet rather than in a low-luminosity nucleus of the galaxy.

Figure 5 also displays the first moment map produced from the spectral-line data cube containing only 10 velocity channels of red-shifted features in Fig 4. A weak velocity gradient, roughly from south to north is seen along the axis  $\text{P.A.} = 155^{\circ}$ . The value of the gradient is, approximately,  $10 \text{ km s}^{-1}$  per  $0.1''$ , or  $2 \text{ km s}^{-1} \text{ pc}^{-1}$ . The gradient is very weak but real, at least from  $554$  to  $563 \text{ km s}^{-1}$ , although the two extrema at the edges  $V_{\text{LSR}} = 564$  and  $553 \text{ km s}^{-1}$  are less certain. However, the zeroth-moment map is well sampled with a good signal-to-noise ratio toward the center portions of the source. As the VLA beam is  $82 \times 77 \text{ mas}$  at  $\text{P.A.} = 6^{\circ}$ , there is no possibility that the gradient along  $\text{P.A.} = 155^{\circ}$  is arising from effects of the beam shape or orientation. Accordingly, I conclude that the observed velocity gradient and its axis are real.

### 3.3. NGC 4051

VLA spectra of the  $\text{H}_2\text{O}$  maser towards the center of NCC4051 (Fig. 6) cover most of the known features in the range  $V_{\text{LSR}} = 640\text{--}780 \text{ km s}^{-1}$ . The location of the systemic feature peaking at  $V_{\text{LSR}} = 717.6 \text{ km s}^{-1}$  is measured at R.A. (J2000)= $12^{\text{h}}03^{\text{m}}09^{\text{s}}.610$ , decl. (J2000)= $+44^{\circ}31'52''.68$ , and all other features are confined to within about  $0.01''$  (or  $0.5 \text{ pc}$ ) from the systemic feature, resulting in the masers being unresolved at this resolution. The beam-deconvolved size of each maser feature is smaller than  $40 \text{ mas}$ , that is, about  $2 \text{ pc}$ . The result is consistent with the earlier VLA-A

snapshot by Hagiwara et al. (2003). Although this new observation has improved  $(u,v)$  coverage over the previous single VLA snapshot, no new useful information is obtained.

## 4. Discussion

### 4.1. M82

#### 4.1.1. $H_2O$ Masers and Luminous X-Ray Sources

The positions of the luminous hard X-ray sources in M82 were measured within an accuracy of  $0.7''$  by *Chandra* (Kaaret et al. 2001; Matsumoto et al. 2001); however, none coincide with those of the  $H_2O$  masers detected in this observation. In addition, there was no high brightness radio source detected at 22 GHz towards any of these luminous X-ray sources, suggesting that these X-ray sources are not likely to be low-luminosity AGNs. Since the masers do not overlap any high-brightness radio sources like an AGN or jet, they are off-nuclear masers that are not directly amplifying the background continuum, as in the case of nuclear  $H_2O$  masers. This is consistent with the fact that the maser luminosity in the galaxy is 1–5 orders of magnitude lower than those of the nuclear  $H_2O$  masers.

#### 4.1.2. $H_2O$ Masers and Other Sources

None of the  $H_2O$  masers detected in this observation are associated with infra-red peaks at  $2.2\mu\text{m}$ , which were considered to be low-luminosity AGN candidates or the dynamical center of the galaxy (Dietz et al. 1986), suggesting that the masers in M82 are not nuclear masers. The separations between each  $H_2O$  maser peak and the center of the nearest continuum source, given in Table 3, indicate that there are no  $H_2O$  masers at the locations of the H II regions or radio SNRs. According to the 5 GHz MERLIN and 15 GHz VLA-PT observations of continuum sources in the galaxy by McDonald et al. (2002), the angular size of each H II region appearing in Table 3 is  $\sim 0.1''\text{--}0.2''$  (2–4 pc) in radius. It is understood that the sizes of Galactic compact H II regions excited by central stars are typically 0.05–0.5 pc and Galactic H II regions are less than  $\sim 5$  pc in radius (e.g., Garay and Lizano 1999). Given the observed separations between the masers and the centers of compact H II regions that range

from  $0.17''$  to  $0.51''$ , corresponding to 3–10 pc, it is less plausible that the masers in the galaxy are directly associated with H II regions or ionizing central stars in the galaxy. In contrast, VLBI observations revealed that the  $H_2O$  maser in the nearby star-forming galaxy M33 is associated with the H II region IC133 (Greenhill et al. 1993). It is thus plausible that some other  $H_2O$  features in M82 might be found in H II regions. The deconvolved angular sizes of RRL emission ( $H92\alpha$ ) in the galaxy displayed in Table 3 range from  $1.4''\text{--}1.7''$  (25–30 pc), just greater than the VLA synthesized beam of  $0.9''$  (Rodriguez et al. 2004) that includes the masers at S1, S2, and N2. The  $H_2O$  maser would not have originated from the RRL -emitting ionized gas, but the RRL marks the prominent star-forming regions in the galaxy, where maser excitation actively occurs.

The velocity deviation of the ionized gas ( $100 - 130 \text{ km s}^{-1}$ ) and molecular gas ( $110 - 145 \text{ km s}^{-1}$ ) from the galaxy’s rigid rotation velocity has been observed, and accounts for the expansion of starburst-driven winds in the galaxy (e.g., Matsushita et al. 2005), but the kinematics connecting the masering clouds with the ionizing medium is not obviously seen from this observation.

#### 4.1.3. What Are the Masers in the Galaxy?

The interpretation of the nature of the  $H_2O$  masers in M82 is not straightforward, since none have distinct continuum counterparts as effective pumping agents. Weiß et al. (1999) imaged an expanding shell-like structure (superbubble) traced by CO and CO isotopes in the galaxy, with a diameter of  $\approx 130$  pc and expansion velocity of  $\sim 45 \text{ km s}^{-1}$ . According to their analysis, the velocity of the approaching side of the expanding shell is  $V_{\text{LSR}} = 95 \text{ km s}^{-1}$  and the receding velocity is  $V_{\text{LSR}} = 190 \text{ km s}^{-1}$ . Thus, the former has an  $H_2O$  maser counterpart at  $V_{\text{LSR}} = 86$  and  $94 \text{ km s}^{-1}$ , but the latter is not covered in this observation. If the maser at S2 is associated with the shell, it could be excited at the shock front of the starburst-driven winds. It is interesting to note that thermal 100 GHz continuum emission has been imaged inside the CO superbubble, and the distribution of the  $H_2O$  masers roughly underlines the continuum emission originating from starburst activity (Matsushita et al. 2005). About 10 OH

main-line masers are observed that are associated with blue-shifted parts of expanding wind-driven shells (Weiß et al. 1999), and the velocities and locations of these OH and H<sub>2</sub>O masers are largely consistent (Pedlar 2005; Matsushita et al. 2005). These OH masers trace the 1667 MHz OH absorption along the major axis of the galaxy, and the OH dynamics understood as solid-body rotation agrees well with the CO emission (Shen & Lo 1995) and H I absorption (Wills et al. 2000). However, there are distinct deviations from this at 350 and  $\sim 70$  km s<sup>-1</sup> (Pedlar et al. 2004), although neither is observed in our observations. Therefore, the detected blue-shifted H<sub>2</sub>O masers are concentrated on the same molecular disk that is traced by OH absorption and CO emission; however, the association of the H<sub>2</sub>O masers with the expanding shells or molecular outflows is not obvious from our data.

Similarly, in the starburst galaxy NGC 253, the locations of low-luminosity H<sub>2</sub>O maser ( $\sim 1 L_{\odot}$ ) are measured towards the nuclear region with the VLA at  $\sim 1''$  resolution (Henkel et al. 2004). The association of the strongest blue-shifted maser features with the RRL, an expanding supernova, or starburst-driven winds is proposed, like the case in M82; however, there is no compelling evidence for that from their observations.

The extent of the CO(2–1) molecular clouds and outflows is not inconsistent with that of the H<sub>2</sub>O maser (Weiß et al. 2001). Molecular outflows in our Galaxy are observed in H<sub>2</sub>O emission, typically on scales of 1–10 AU, which is at least 100 times smaller than the masers measured on the parsec-scale with the VLA. Accordingly, even if the masers probed part of the outflow, they would not be resolved on these scales by analogy with the cases of young stellar objects (YSOs) in our Galaxy. It is believed that H<sub>2</sub>O masers indicate sites of star-formation and appear at a certain stage of the evolutionary history of proto-stars. It is also understood that CH<sub>3</sub>OH, OH, and H<sub>2</sub>O masers are observed at different evolutionary stages of star formation, and H<sub>2</sub>O emerges at the earliest stage of massive star formation during the rapid accretion phase (Churchwell 2002). Masers in a galaxy that do not accompany compact H II regions and OH masers may be the signposts of the early stage of star formation and are most likely to be associated with molecular outflows or accretion

disks around extra-galactic YSOs that have not been studied to date (e.g., Torrelles et al. 1998).

## 4.2. M51

### 4.2.1. Blue-shifted Features

The precise location of the known weak and variable blue-shifted features lying from  $V_{\text{LSR}} = 435\text{--}445$  km s<sup>-1</sup> in this galaxy (Hagiwara et al. 2001) has been an open question. One of them has been pinpointed in this observation for the first time. Taking the fact that the maser luminosity of the blue-shifted emission is approximately  $0.17 L_{\odot}$  from the VLA spectrum and is not associated with any known radio continuum sources in the galaxy, one can infer that AGN activity is not the major source giving rise to the maser. The blue-shifted emission is displaced  $1.7''$ , or 82 pc, from the red-shifted counterpart near the nucleus, thus, no hint of physical connection exists between these velocity clusters. From what do the features arise? The peak velocity of  $V_{\text{LSR}} = 445$  km s<sup>-1</sup> is in the velocity range of the central HCN emission (Kohno et al. 1996). The features lie in the central dense region of the HCN emission, where the mean velocity field of the HCN emission is  $V_{\text{LSR}} \sim 480$  km s<sup>-1</sup>, that is,  $35$  km s<sup>-1</sup> shifted from the maser (Kohno et al. 1996). Thus, it is impossible to find common mechanics connecting the two different velocity gradients traced by the maser and the HCN. All that one can speculate is that the maser traces the most dense part ( $\gtrsim 10^7$  cm<sup>-3</sup>) of the circumnuclear molecular gas within 10 pc of the nucleus. As a result of this observation, the bipolar-jet model proposed in Hagiwara et al. (2001), in which the blue-shifted features are associated with the approaching side of the jet, is no longer eligible.

### 4.2.2. Central Kinematics

One of the most exciting results from this observation is that part of the velocity structure of the dense molecular gas within a few parsecs of the nucleus is resolved at sub-arcsecond resolution. The detected velocity gradient is about  $2$  km s<sup>-1</sup> pc<sup>-1</sup>, and the direction of the gradient (PA  $\sim 155^\circ$ ) is similar to that of the radio jet but not to the rotational axis of the inner torus with a radius of 70 pc (PA  $\sim 160^\circ\text{--}165^\circ$ ) postulated from the distribution of the HCN ( $J = 1\text{--}0$ ) emission observed

at 4" resolution (Kohno et al. 1996). Most of the red-shifted maser features in Fig. 4 are neither in the velocity range of CO ( $J = 1-0$ ) ( $V_{\text{LSR}} = 387-547 \text{ km s}^{-1}$ ) nor in that of HCN ( $J = 1-0$ ) ( $V_{\text{LSR}} = 377-546 \text{ km s}^{-1}$ ). The velocity ranges of the maser do not agree with those of the HCN emission and the HCN torus model proposed in Kohno et al. (1996), however, the axis of the HCN torus is not inconsistent with the direction of the maser velocity field.

Given the fact that the blue-shifted features are separated by  $\sim 80 \text{ pc}$  from the rest of the features, and do not coincide with the nucleus, the whole maser system is unlikely to trace a subparsec-scale Keplerian disk observed with the nuclear  $\text{H}_2\text{O}$  maser, if it exists. However, it is possible that only the red-shifted features trace a part of a rotating disk, and the blue-shifted features on the disk are invisible. Assuming that the observed maser is on a disk at a radius  $r$  from the nucleus and with a rotating velocity of  $V_{\text{rot}}$ , the observed velocity gradient ( $dV/dl$ ) along P.A. =  $155^\circ$  can be expressed as  $dV/dl \simeq d(V_{\text{rot}} \theta \sin i)/d(r\theta) = V_{\text{rot}}/r$ , where  $l$  is the projected distance,  $i$  is the disk inclination, and the approximation of  $\sin\theta \approx \theta$  is made. Adopting the disk inclination of  $80^\circ$  from the edge-on circumnuclear-nuclear disk with a radius of  $70 \text{ pc}$  (Kohno et al. 1996), together with the observed parameters of  $dV/dl = 2 \text{ km s}^{-1} \text{ pc}^{-1}$  and  $V_{\text{red}} - V_{\text{sys}} = V_{\text{rot}} \simeq 100 \text{ km s}^{-1}$ ,  $r$  is estimated to be  $50 \text{ pc}$ . The result suggests that the observed maser probes a disk on a scale of  $10 \text{ pc}$  but not a thin disk with  $r < 0.1 \text{ pc}$ , such as the one in NGC 4258 (e.g. Herrnstein et al. 1998).

Does the maser disk lie in an inner part of the circumnuclear HCN disk? Taking this value for the radius of a molecular disk, the mass confined within the disk is  $1.2 \times 10^8 M_\odot$ , that is, 1 or 2 mag larger than the molecular hydrogen and dynamical mass within  $r < 70 \text{ pc}$ , based on the estimation from the HCN intensities (Kohno et al. 1996). Accordingly, we cannot account for the detected velocity field with a subparsec-scale masering disk or a larger scale molecular disk.

It is interesting to note that the velocity gradient of  $0.65 \text{ km s}^{-1} \text{ pc}^{-1}$  along the radio jet axis was detected in CO( $J = 3-2$ ) at 4" resolution ( $\sim 160 \text{ pc}$ ) using the Submillimeter Array by Matsushita et al. (2004), although the sampled area in their image is more than 100 times larger

than that in this VLA observation. The CO velocity gradient in their position-velocity map covers that of the maser at  $V_{\text{LSR}} = 555-565 \text{ km s}^{-1}$ . However the observed CO gradient is more dominant in the direction perpendicular to the jet, and such a small velocity gradient in the thermally excited molecular gas is likely due to the internal turbulence, as also mentioned in Matsushita et al. (2004). Thus, there is no compelling evidence that the maser and CO( $J = 3-2$ ) trace the same kinematics, but both of them could be distributed in the same molecular cloud. In the VLBI observation of the 1667 MHz OH maser towards the type 1 Seyfert nucleus in Mrk 231, a weak velocity gradient of  $1.4 \text{ km s}^{-1} \text{ pc}^{-1}$  across the torus structure with a radius of  $65 \text{ pc}$  is reported in OH emission (Klöckner et al. 2003), which does not agree with any thermal molecular gas structure. In this sense, the OH maser in Mrk 231 is similar to the  $\text{H}_2\text{O}$  maser in M51. The axis of the OH torus in Mrk 231 is not aligned with the major axis of the nuclear continuum source; rather, it is perpendicular to the nuclear continuum axis. This is different from the case of M51, in which the velocity field of the maser is almost aligned with the jet axis, which might rule out the presence of a masering disk in the galaxy. Note that there are still some other blue-shifted features whose positions have not yet been pinned down, some of which could be on a masering torus within  $1 \text{ pc}$  from the center, along with red-shifted counterparts. If the maser in M51 is resolved down to scales of  $0.1 \text{ pc}$  using VLBI, the velocity structures of the maser will be interpreted differently. The most plausible explanation for the maser and its velocity gradient based on these observations is that the maser arises in a dense molecular environment in the foreground of a radio jet, amplifying the background radio continuum jet (Claussen et al. 1998), or, alternatively is from a shocked dense region near the boundary of the jet (Hagiwara et al. 2001). The weak radio intensity of the jet would account for the low luminosity of the maser.

### 4.3. NGC4051

The luminosity of the  $\text{H}_2\text{O}$  maser in NGC 4051 is  $\sim 1 L_\odot$ , very low for nuclear masers. It might appear that such a low-luminosity maser is not related to direct AGN activity. However, Hagiwara et al. (2003) proposed that the

low-luminosity of the maser and narrower total velocity span of the Doppler-shifted features ( $\sim 100 \text{ km s}^{-1}$ ) might be due to low-gain maser amplification, resulting from a small inclination of a disk-like structure surrounding the AGN. Hagiwara et al. (2003) hypothesized that the maser originated from a less edge-on disk-like configuration surrounding a nucleus, which would cause relatively short gain paths in the line of sight. This could account for the low-luminosity of the maser. Madejski et al. (2006), however, argue that the maser in NGC 4051 is unlikely to be connected with direct AGN activity, in that the X-ray absorbing medium is significantly ionized in NGC 4051, and such an ionized absorbing medium is unlikely to be physically close to the masering medium. They suggest that the origin of the maser in NGC 4051 is in nuclear winds, because the broadly spread ( $\sim 280 \text{ km s}^{-1}$ ) narrow -line spectrum is similar to that of the Circinus galaxy. Circinus hosts highly Doppler-shifted maser features with a total velocity range of  $\sim 160 \text{ km s}^{-1}$  that are introduced as nuclear wind components, together with features tracing an edge-on disk with a sub-Keplerian rotation (Greenill et al. 2003). However, a physical mechanism driving the nuclear winds in the galaxy has not yet been proposed.

One can speculate that the medium giving rise to the maser is geometrically separated from the X-ray absorber. The inner edge of the absorber could be illuminated by direct X-ray radiation and hence ionized, which would also cause a high time variability of the X-ray-measured column density  $N_H$ , while the masering medium could exist in the outer edge of a thin disk that is much less ionized because of a large radial distance from the X-ray heating source. The known periodic intensity variability at hard X-ray bands might occur in the inner edge of the disk (e.g., Herrnstein et al. 1998), while the time-interval of the intensity variability of the maser is very different. In the case of NGC 4388, the radius of the absorbing medium is estimated from the variability of  $N_H$  to be a few hundred Schwarzschild radii ( $R_{\text{sch}}$ ) (Elvis et al. 2004), that is 100 times smaller than the (sub-)parsec-scale obscuring medium observed in the  $\text{H}_2\text{O}$  maser.  $\text{H}_2\text{O}$  masers in NGC 4258 are distributed in a region between 40,000 and 80,000

$R_{\text{sch}}$  from the nucleus (e.g., Herrnstein et al. 1998). Therefore, it is less plausible that the masering medium and X-ray-ionizing structure occur in a single physical structure. Thus, we still cannot rule out the presence of a maser disk in NGC 4051. In any case, the hypothesis proposed by Hagiwara et al. (2003) should be tested at milliarcsecond angular resolutions by resolving the maser distribution on scales of 0.1 pc or less.

## 5. FAR-INFRARED VS RADIO INTENSITY CORRELATION DIAGRAM

There is a known strong linear correlation between the far-infrared (FIR) flux density and the radio flux density at 1.4 GHz from nuclear starburst galaxies (Helou et al. 1985; Condon et al. 1991), which implies that FIR radiation and non-thermal radio emission at 1.4 GHz are closely connected with star-forming activity. In Fig 7 there are three different comparisons: the ratios of the 1.4 GHz radio fluxes to FIR flux from high-luminosity  $\text{H}_2\text{O}$  masers, as well as from low-luminosity  $\text{H}_2\text{O}$  masers and prototypical OH megamasers (OHMMs) from ultra-luminous FIR galaxies. The low-luminosity masers and OHMM samples follow well the known FIR-radio correlation. The mean constant ratios of these three samples are also displayed in Fig 7, from which one can see that the ratio for the low-luminosity masers is steeper than those of the other two. The reason for this deviation is that the FIR fluxes are relatively more dominant for the low-luminosity masers, which supports the idea that the low-luminosity masers are powered by star-forming activity rather than AGN activity. We cannot discriminate the synchrotron emission at 1.4 GHz from either SNR or AGN ejecta, but the FIR emission is characterized as re-emission from the dust heated by starburst/star-forming activity (e.g., Hagiwara et al. 2002). It is interesting to note that there is a population of high-luminosity masers that shows a higher ratio of the radio to FIR fluxes in the bottom phase-space in the diagram, which may suggest a close connection of maser excitation to strong radio flux from AGN activity.

## 6. SUMMARY

Low-luminosity extragalactic H<sub>2</sub>O masers have been identified in different physical environments related to star-formation, such as H II regions, YSOs, or possibly SNRs. Given the fact that the luminosity of the strongest Galactic H<sub>2</sub>O maser, W49N, is  $\sim 1 L_{\odot}$ , the origin of these low-luminosity masers can be explained by star-forming activity in their host galaxies. Many of the host galaxies of these masers contain star-forming regions or exhibit starburst activity but do not contain an AGN. These H<sub>2</sub>O masers may reveal new stellar phenomena relevant to extragalactic star-forming activity.

The kinematics of H<sub>2</sub>O masers in M82 is broadly consistent with OH or CO solid body rotation along the galaxy's major axis, but locally the masers are not associated with any other molecular emission. Including the three new detections, the masers are not directly associated with any continuum sources, such as compact H II regions or radio SNRs, suggesting that the masers arise from the earliest stage of star-forming activity in the galaxy. For the masers in M51, the detected blue-shifted features are significantly offset from the nuclear radio continuum, while the red-shifted counterparts are in the nuclear radio source. Seemingly, the maser in the galaxy amplifies the radio jet continuum, which needs to be confirmed at higher resolution. The most remarkable result is that a small velocity gradient roughly along the jet has been detected from red-shifted emission at 0.1" resolution. However, the interpretation of the velocity gradient is not straightforward. The nature of the maser in NGC4051 is controversial and also needs to be studied at higher resolutions. A study of the distribution of the rare H<sub>2</sub>O masers towards a NLS1 showing a low accretion rate and hence a smaller black hole mass is of great interest. According to a statistical study, it is found that the mean FIR-to-radio flux ratio of low-luminosity H<sub>2</sub>O masers is higher than that of their high-luminosity counterparts, suggesting that the maser excitation of low-luminosity water masers such as the one in M82 is related primarily to star-forming activity, rather than AGN activity.

I would like to thank the anonymous referee for

a number of useful comments on the manuscript. I am grateful to the NRAO staff for their assistance during data analysis. This research is based on observations with the 100m telescope of the Max-Planck-Institut für Radioastronomie at Effelsberg. This research has made use of the NASA/IPAC Extragalactic Database, which is operated by the Jet Propulsion Laboratory, California Institute of Technology, under contract with the National Aeronautics and Space Administration.

## REFERENCES

- Adams, T. F. 1977, *ApJS*, 33, 19
- Argo, M. K., Pedlar, A., Muxlow, T. W. B., et al., 2004, in proceedings of the 7th Symposium of the European VLBI Network (Toledo), ed. R. Bachiller, et al. (Observatorio Astronomico Nacional of Spain), 151
- Baudry, A., & Brouillet, N. 1996, *A&A*, 316, 188
- Braatz, J. A., Henkel, C., Greenhill, L. J., Moran, J. M., & Wilson, A. S. 2004, *ApJ*, 617, L29
- Bradley, L. D., Kaiser, M. E., & Baan, W. A. 2004, *ApJ*, 603, 463
- Churchwell, E., Witzel, A., Huchtmeier, W., Pauliny-Toth, I., Roland, J., & Sieber, W. 1977, *A&A*, 54, 969
- Churchwell, E. 2002, *ARA&A*, 40, 27
- Claussen, M. J., Diamond, P. J., Braatz, J. A., Wilson, A. S., & Henkel, C. 1998, *ApJ*, 500, L129
- Claussen, M. J., Heiligman, G. M., & Lo, K. Y. 1984, *Nature*, 310, 298
- Condon, J. J., Anderson, M. L., & Helou, G. 1991, *ApJ*, 376, 95
- Dietz, R. D., Smith, J., Hackwell, J. A., Gehrz, R. D., & Grasdalen, G. L. 1986, *AJ*, 91, 758
- Dos Santos, P. M., & Lépine, J. R. D. 1979, *Nature*, 278, 34
- Elvis, M., Risaliti, G., Nicastro, F., Miller, J. M., Fiore, F., & Puccetti, S. 2004, *ApJ*, 615, L25

- Freedman, W. L., Hughes, S. M., Madore, B. F., et al. 1994, *ApJ*, 427, 628
- Garay, G., & Lizano, S. 1999, *PASP*, 111, 1049
- Greenhill, L. J., Moran, J. M., Reid, M. J., et al. 1990, *ApJ*, 364, 513
- Greenhill, L. J., Moran, J. M., Reid, M. J., Menten, K. M., & Hirabayashi, H. 1993, *ApJ*, 406, 482
- Greenhill, L. J., et al. 2003, *ApJ*, 590, 162
- Hagiwara, Y., Henkel, C., Menten, K., & Nakai, N. 2001, *ApJ*, 560, L37
- Hagiwara, Y., Diamond, P. J., & Miyoshi, M. 2002, *A&A*, 383, 65
- Hagiwara, Y., Diamond, P. J., Miyoshi, M., Rovi-  
los, E., & Baan, W. 2003, *MNRAS*, 344, L53
- Helou, G., Soifer, B. T., & Rowan-Robinson, M. 1985, *ApJ*, 298, L7
- Henkel, C., Braatz, J. A., Greenhill, L. J., & Wilson, A. S. 2002, *A&A*, 394, L23
- Henkel, C., Tarchi, A., Menten, K. M., & Peck, A. B. 2004, *A&A*, 414, 117
- Henkel, C., Peck, A. B., Tarchi, A., Nagar, N. M., Braatz, J. A., Castangia, P., & Moscadelli, L. 2005, *A&A*, 436, 75
- Herrnstein, J. R., Greenhill, L. J., Moran, J. M., Diamond, P. J., et al. 1998, *ApJ*, 497, L69
- Ho, P. T. P., Martin, R. N., Henkel, C., & Turner, J. L. 1987, *ApJ*, 320, 663
- Kaaret, P., Prestwich, A. H., Zezas, A., Murray, S. S., Kim, D.-W., Kilgard, R. E., Schlegel, E. M., & Ward, M. J. 2001, *MNRAS*, 321, L29
- Klößner, H.-R., Baan, W. A., & Garrett, M. A., 2003, *Nature*, 421, 821
- Kohno, K., Kawabe, R., Tosaki, T., & Okumura, S. K. 1996, *ApJ*, 461, L29
- Kondratko, P.T., et al. 2006, *ApJ*, 638,100
- Lawrence, A., Watson, M. G., Pounds, K. A., & Elvis, M. 1987, *Nature*, 325, 694
- Madejski, G., Done, C., Życki, P. T., & Greenhill, L. 2006, *ApJ*, 636, 75
- Matsumoto, H., Tsuru, T. G., Koyama, K., et al. 2001, *ApJ*, 547, L25
- Matsushita, S., et al. 2004, *ApJ*, 616, L55
- Matsushita, S., Kawabe, R., Kohno, K., Matsumoto, H., Tsuru, T. G., & Vila-Vilaró, B. 2005, *ApJ*, 618, 712
- McDonald, A. R., Muxlow, T. W. B., Wills, K. A., Pedlar, A., & Beswick, R. J. 2002, *MNRAS*, 334, 912
- Osterbrock, D. E., & Pogge, R. W., 1985 *ApJ*, 297, 166
- Pedlar, A., Muxlow, T. W. B., Smith, R. et al. 2004, in *ASP Conference Series 320, The Neutral ISM in Starburst Galaxies*, ed. S. Aalto, S. Hüttemeister, & A. Pedlar, 183
- Pedlar, A. 2005, *Ap&SS*, 295, 161
- Rodriguez-Rico, C. A., Viallefond, F., Zhao, J. -  
H., Goss, W. M., & Anantharamaiah, K. R. 2004, *ApJ*, 616, 783
- Sandage, A., & Tammann, G. A. 1975, *ApJ*, 196, 313
- Sanders, D. B., Soifer, B. T., Elias, J. H., Madore, B. F., Matthews, K., Neugebauer, G., & Scoville, N. Z. 1988, *ApJ*, 325, 74
- Scoville, N., & Young, J. S. 1983, *ApJ*, 265, 148
- Scoville, N. Z., Yun, M. S., Armus, L., Ford, H. 1998, *ApJ*, 493, L63
- Seaquist, E. R., Frayer, D. T., & Frail, D. A. 1997, *ApJ*, 487, L131
- Shen, J., & Lo, K. Y. 1995, *ApJ*, 445, L99
- Singh, K. P. 1999, *MNRAS*, 309, 991
- Tarchi, A., Henkel, C., Peck, A. B., & Menten, K. M. 2002a, *A&A*, 385, 1049
- Tarchi, A., Henkel, C., Peck, A. B., & Menten, K. M. 2002b, *A&A*, 389, L39
- Torrelles, J. M., Gómez, J. F., Rodríguez, L. F., et al. 1998, *ApJ*, 505, 756

- Ulvestad J. S., Wilson A. S. 1984, ApJ, 285, 439
- Weiß, A., Walter, F., Neiningen, N., Klein, U. 1999, A&A, 345, 23L
- Weiß, A., Neiningen, N., Hüttemeister, S., & Klein, U. 2001, A&A, 365, 571
- Williams, R. J., Mathur, S., & Pogge, R. W. 2004, ApJ, 610, 737
- Wills, K. A., Das, M., Pedlar, A., et al. 2000, MNRAS, 316, 33

TABLE 1  
SUMMARY OF VLA OBSERVATIONS

Object ( <i>Cal. Source</i> )	Date (d.m.y)	Tracking-Center		Velocity Range (km s <sup>-1</sup> )	$\Delta V^a$ (km s <sup>-1</sup> )	$t^b$ (hr)	Beam (HPBW) (mas)	$\sigma_{\text{rms}}$ (mJy beam <sup>-1</sup> )
		R.A. (h m s)	Decl. ( <sup>o</sup> ' '' )					
M82	13.4.02	$\alpha_{1950}$ 09 51 42.200	$\delta_{1950}$ 69 54 59.30	50-130 70-150	1.3	9	93×80 PA=45°	1.1
(0955+654)	-	09 54 57.847	65 48 15.53	-	-	-	-	-
M51	4.7.03	$\alpha_{2000}$ 13 29 52.708	$\delta_{2000}$ 47 11 42.79	365-525 480-640	5.3	8	82×77 PA=6°	1.1
(1419+542)	-	14 19 46.597	54 23 14.78	-	-	-	-	-
NGC4051	4.7.03	$\alpha_{2000}$ 12 03 09.606	$\delta_{2000}$ 44 31 52.52	640-725 695-780	1.3	9	77×72 PA=81°	1.3
(1153+493)	-	11 53 24.466	49 31 08.83	-	-	-	-	-

\*Equinox for M82 is B1950.0; equinox for M51 and NGC4051 is J2000.0.

<sup>a</sup>Velocity resolution

<sup>b</sup>Total observing time

TABLE 2  
H<sub>2</sub>O MASER IN M82

Component	$\alpha_{B1950}$ (09 <sup>h</sup> 51 <sup>m</sup> 00 <sup>s</sup> )	$\delta_{B1950}$ (69°54'00'')	Peak Flux (mJy)	Velocity (km s <sup>-1</sup> ,LSR)	Feature Width <sup>a</sup> (Channel)	L <sub>H<sub>2</sub>O</sub> (L <sub>⊙</sub> )
S1 <sup>b</sup>	42.6476 ± 0.0006	58.180 ± 0.003	13	126	2	0.008
S2 <sup>b</sup>	42.1808 ± 0.0002	59.263 ± 0.001	63	108	3	0.062
	42.1799 ± 0.0007	59.257 ± 0.004	15	98	1	0.006
	42.1825 ± 0.0014	59.252 ± 0.007	8	84	1	0.003
N1	42.3951 ± 0.0012	58.195 ± 0.007	8	105	4	0.007
N2	40.9436 ± 0.0007	58.756 ± 0.004	16	146	1	0.006
N3	41.2053 ± 0.0014	59.602 ± 0.007	5	98	1	0.002

<sup>a</sup>Each channel is 1.3 km s<sup>-1</sup> wide.

<sup>b</sup>Adopting labels in Baudry & Brouillet (1996)

TABLE 3  
H<sub>2</sub>O MASER AND OTHER SOURCES IN M82

H <sub>2</sub> O Maser (Position ID)	Nearest Discrete Continuum <sup>a</sup>			Origin <sup>a</sup> (09 <sup>h</sup> 51 <sup>m</sup> 00 <sup>s</sup> )	Nearest H92 <sub>α</sub> <sup>b</sup> RRL	
	$\alpha_{B1950.0}$ (09 <sup>h</sup> 51 <sup>m</sup> 00 <sup>s</sup> )	$\delta_{B1950.0}$ (69°54'00'')	$\theta_{\text{sep}}^c$ (arcsec)		$\alpha_{B1950.0}$ (69°54'00'')	$\delta_{B1950.0}$
S1(42.64+58.1)	42.694	58.24	0.31	H <sub>II</sub>	42.61	58.0
S2(42.18+59.2)	42.210	59.04	0.22	H <sub>II</sub>	42.19	58.8
N1(42.39+58.2)	42.481	58.36	0.49	H <sub>II</sub>		
N2(40.94+58.7)	40.938	58.87	0.17	H <sub>II</sub>	40.97	58.5
N3(41.20+59.6)	41.302	59.64	0.51	SNR		

<sup>a</sup>McDonald et al. (2002)

<sup>b</sup>Rodriguez et al. (2004)

<sup>c</sup>Angular distance between each maser spot and the nearest continuum source.

TABLE 4  
H<sub>2</sub>O MASER IN M51

Component	$\alpha_{J2000.0}$ (13 <sup>h</sup> 29 <sup>m</sup> 00 <sup>s</sup> )	$\delta_{J2000.0}$ (47° 11' 00'')	Peak Flux (mJy)	Velocity (km s <sup>-1</sup> , LSR)	Feature Width <sup>a</sup> (Channel)	L <sub>H<sub>2</sub>O</sub> (L <sub>⊙</sub> )
Blue-shifted component	52.5486 ± 0.0016	43.337 ± 0.012	8.2	445	2	0.1
Red-shifted components	52.7089 ± 0.0001	42.790 ± 0.001	41.8	539	1	0.47
	52.7087 ± 0.0001	42.789 ± 0.001	52.6	565	1	0.58
	52.7091 ± 0.0001	42.788 ± 0.002	23.4	576	1	0.26

<sup>a</sup>Each channel is 5.3 km s<sup>-1</sup> wide.

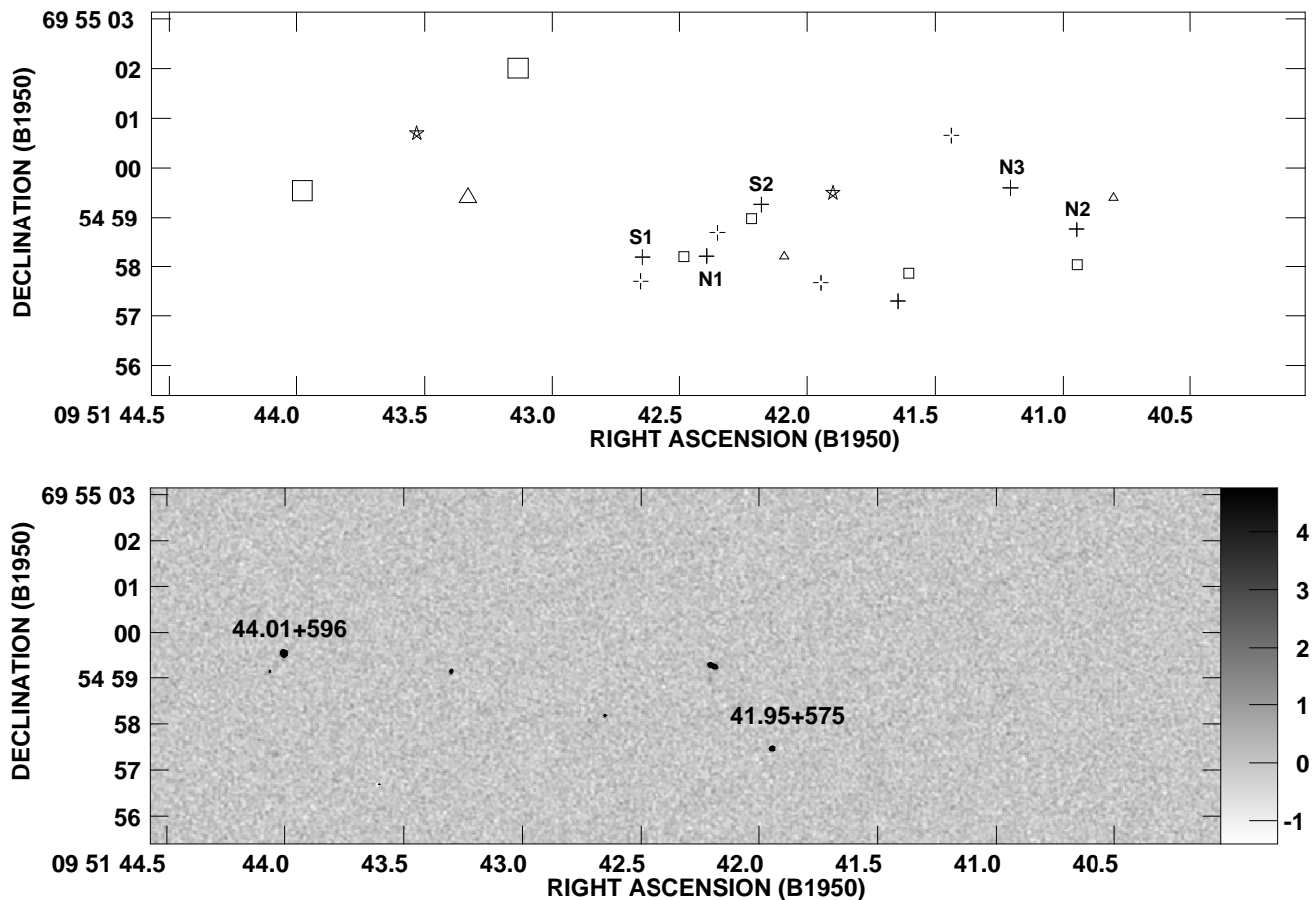


Fig. 1.— *Top*: Locations of H<sub>2</sub>O masers, with other emission shown for comparison, in M82. Infra-red continuum peaks at 2.2  $\mu\text{m}$  (Dietz et al. 1986) are plotted with stars, H<sub>2</sub>O masers are by crosses, 1667/1665 MHz OH masers (Argo et al. 2004) are shown by squares, 1720 MHz OH masers (Seaquist et al. 1997) are shown by triangles, and hard X-ray points are shown by broken crosses (Kaaret et al. 2001; Matsumoto et al. 2001). Larger squares and triangles indicate blue-shifted emission relative to 200 km s<sup>-1</sup>; their smaller counterparts show red-shifted ( $V_{\text{LSR}} > 200$  km s<sup>-1</sup>) emission. The systemic velocity of the galaxy is  $220 \pm 5$  km s<sup>-1</sup>. It is obvious that all of the locations of OH and H<sub>2</sub>O masers are well separated in space, depending on their offset relative to the velocity of 200 km s<sup>-1</sup>. *Bottom*: The 1.3-cm radio continuum version of the map shown in the top panel. Gray-scales are plotted from -1.0 to 5.0 mJy beam<sup>-1</sup>.

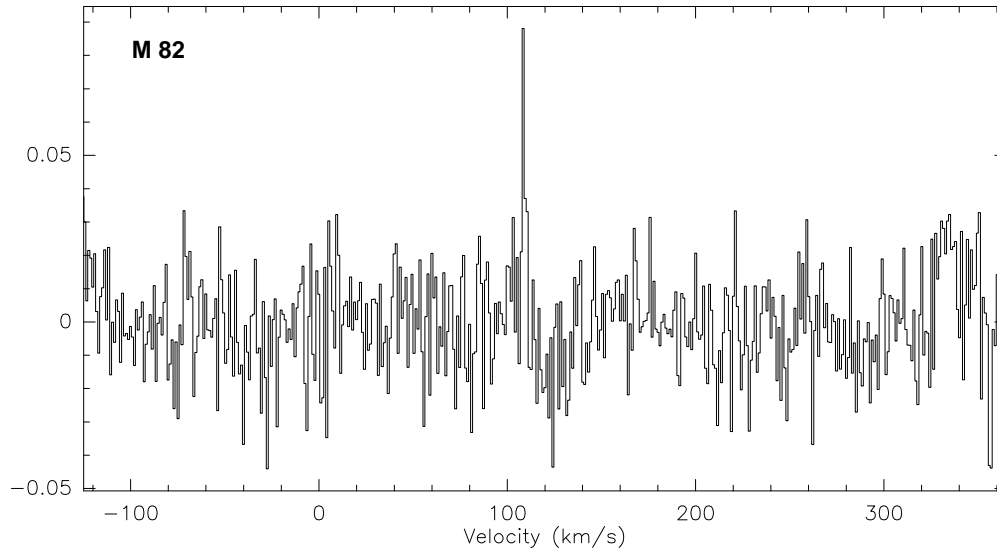


Fig. 2.— Single-dish spectrum of the H<sub>2</sub>O maser towards the center of M82. The velocity resolution is 1.1 km s<sup>-1</sup>. The total integration time is ~ 60 minutes, observed with the MPIfR 100 m telescope at Effelsberg on 7 March 2002. The amplitude is scaled in janskys.

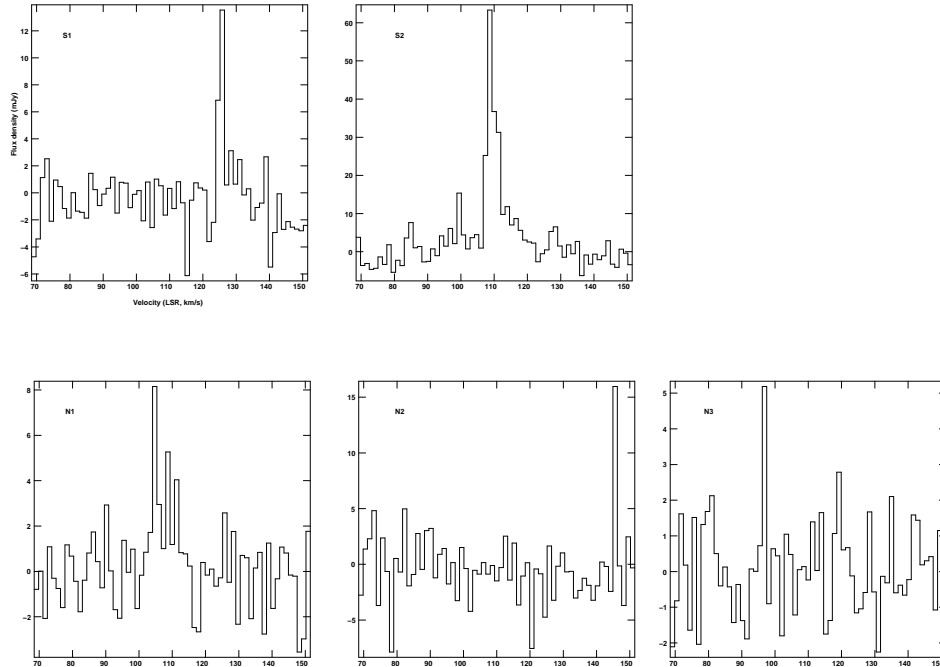


Fig. 3.— VLA H<sub>2</sub>O maser spectra towards five locations in M82 within  $V_{\text{LSR}} = 70 - 150 \text{ km s}^{-1}$ . The masers towards S1 and S2 were originally detected at 1'' resolution of the VLA (Baudry & Brouillet 1996). Their positions are constrained at 0.1'' resolution in this paper. The masers at N1, N2, and N3 are new detections.

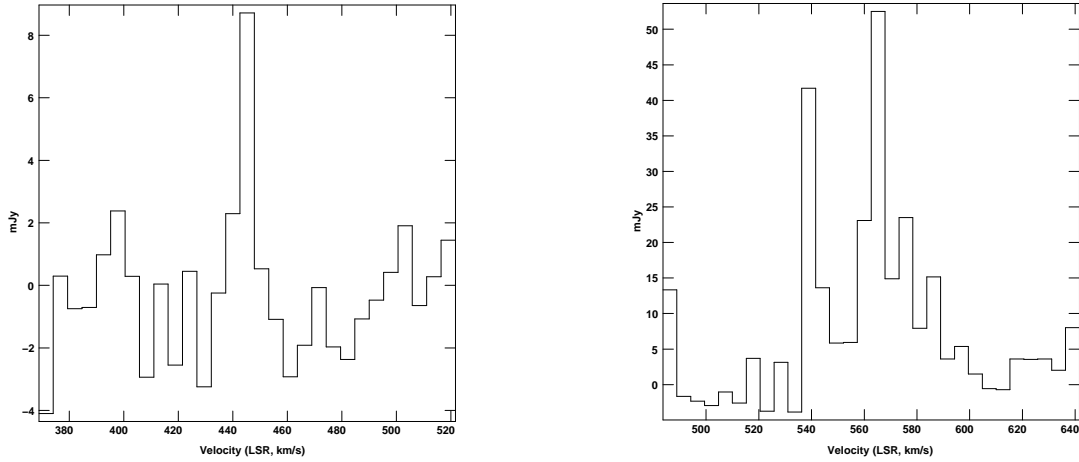


Fig. 4.—  $\text{H}_2\text{O}$  maser spectra of M51, observed with VLA-A on 4 July 2003. The left panel covers blue-shifted velocity range, and the right panel covers the red-shifted range. The velocity resolution is  $5.3 \text{ km s}^{-1}$ . The spectra were obtained from two IF channels, each with 12.5 MHz bandwidth.

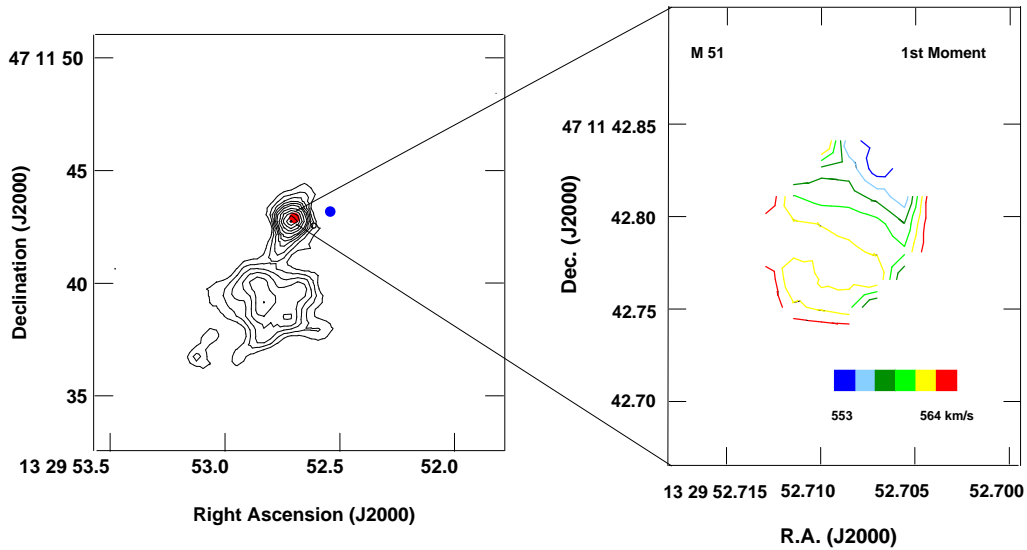


Fig. 5.— *Left*: Large-scale 8.4 GHz nuclear continuum of M51 imaged by the VLA (Bradley, Kaiser, & Baan 2004), superposed with two approximate positions of the  $\text{H}_2\text{O}$  maser. The red-shifted cluster is marked in red in the vicinity of the continuum peak and the blue-shifted feature(s) marked in blue is offset from both the peak and the other maser cluster. *Right*: First velocity moment map of the red-shifted maser from the uniform-weight map. A small velocity gradient over the maser is identified. Contours are spaced at 1–2  $\text{km s}^{-1}$  and labeled with the absolute LSR velocity-scale.

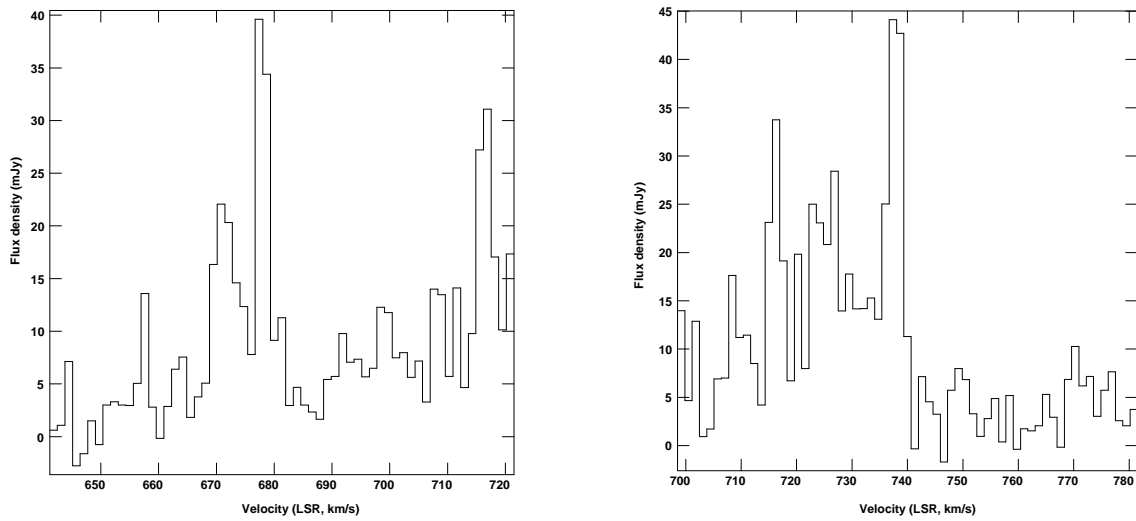


Fig. 6.— H<sub>2</sub>O maser spectra from the nucleus of NGC 4051 with a velocity resolution of  $1.3 \text{ km s}^{-1}$  using the VLA. The spectra consist of two independent IF channels that cover the velocity range of  $V_{\text{LSR}} = 640\text{--}780 \text{ km s}^{-1}$ , straddling the systemic velocity of  $V_{\text{LSR}} = 730 \text{ km s}^{-1}$ .

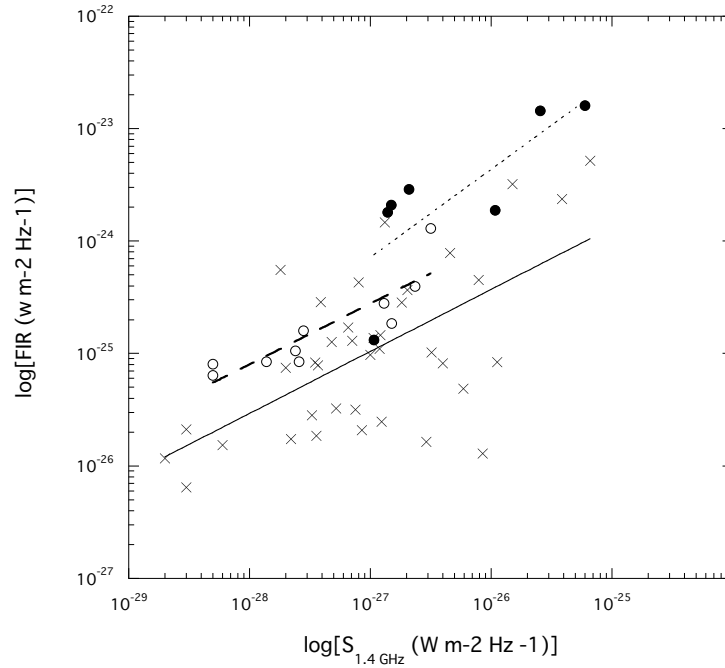


Fig. 7.— The 1.4 GHz radio flux density vs. FIR flux density (estimated from  $60\ \mu\text{m}$  and  $100\ \mu\text{m}$ ). Crosses represent the known high-luminosity water masers in the literature, and filled circles represent low-luminosity water masers in star-forming nuclei (IC10, IC342, M51, M82, NGC253, NGC2146, and NGC6946), primarily from Greenhill et al. (1990); Tarchi et al. (2002a,b); Henkel et al. (2002); Claussen et al. (1984). Open circles represent prototypical OHMMs from Sanders et al. (1988). Mean constant ratios of FIR to 1.4 GHz radio flux densities for the three different samples are indicated by the solid line (high-luminosity  $\text{H}_2\text{O}$  maser), the dashed line (OHMM), and the dotted line (low-luminosity  $\text{H}_2\text{O}$  maser).